Backward-Wave Cancellation in Distributed Traveling-Wave Photodetectors

Sanjeev Murthy, *Student Member, IEEE*, Seong-Jin Kim, Thomas Jung, *Student Member, IEEE*, Zhi-Zhi Wang, Wei Hsin, T. Itoh, *Life Fellow, IEEE*, and Ming C. Wu, *Fellow, IEEE, Member, OSA*

Invited Paper

Abstract—This paper describes the design, fabrication, and measurement of backward-wave-cancelled distributed traveling-wave photodetectors. One of the fundamental issues in traveling-wave photodetectors is the generation of backward-waves, which reduces bandwidth or, in the case of matched input termination, reduces their radio-frequency (RF) efficiencies by up to 6 dB. We report a traveling-wave photodetector with multisection coplanar strip transmission lines. The reflections at the discontinuities of the transmission line cancel the backward propagating waves exactly. The bandwidth reduction due to backward-waves is eliminated without sacrificing the RF efficiency. We have demonstrated a broadband backward-wave-cancelled traveling-wave photodetector with three discrete photodiodes. The photodetector is realized in InGaAs/InGaAsP/InP material systems and operates at 1.55 μm. A 3-dB bandwidth of 38 GHz and a linear RF output of -1 dBm at 40 GHz have been achieved. The experimental results agree very well with the theoretical calculations.

Index Terms—Backward-wave cancellation, coplanar transmission line, distributed photodetectors, high-power photodetectors, microwave photonics, traveling-wave photodetectors, velocity matched distributed photodetectors.

I. INTRODUCTION

TRAVELING-WAVE photodetectors (TWPDs) have attracted much attention recently [1]–[12]. The speed of conventional lumped element photodetectors is limited by RC time and carrier transit time. By embedding the photodetector in a microwave transmission line, the capacitance of the photodiode becomes part of the distributed capacitance of the transmission line, and the RC time associated with the line impedance and the diode capacitance is eliminated. This enables us to build photodetectors with higher speed, or, perhaps more importantly, high-speed photodetectors with large absorption volume for high power operation. There are two main applications of TWPDs: the first is generation of widely tunable millimeter and submillimeter waves or even

terahertz radiations by photomixing techniques [13]; the other is linear photodetectors with high saturation photocurrent for analog fiber optic links or radio-frequency (RF) photonic systems. High-power high-speed photodetectors reduce RF insertion loss and increase spurious-free dynamic range and signal-to-noise ratio of analog fiber optic links [13], [14].

There are two types of TWPDs. The simpler type has a continuous absorption region along the microwave transmission line [1]–[4], [6], [12]. For continuous TWPD with p-i-n structures, the phase velocity of the microwave transmission line is lower than that of the optical waves due to excessive capacitive loading from the photodiode [6]. To avoid the bandwidth limit due to the walkoff (or velocity mismatch) between the optical and the microwave signals, the lengths of continuous TWPDs are generally much shorter than the wavelength of the RF signals. The impedance of continuous TWPD is usually lower than 50 Ω due to the same capacitive loading. The second type of TWPDs, called velocity-matched distributed photodetectors (VMDP) or periodic TWPD, divides the absorption length into discrete photodiodes connected by a passive optical waveguide [5], [7], [10], [11]. The microwave and the optical velocities in VMDP can be matched by adjusting the sizes and separation of the discrete photodiodes. It is also possible to design a transmission line with a 50-Ω impedance in VMDP. Both types of TWPDs offer higher power handling capabilities than lumped photodetectors. The maximum photocurrents are limited by catastrophic damage caused by thermal run away process [15]. The TWPDs have lower thermal impedances because the heat generated by the photocurrents is distributed over a larger area. Even lower thermal impedance can be obtained in VMDP with large diode spacing (more than the thickness of the substrate).

One of the fundamental issues for traveling-wave photodetectors is the backward propagating waves generated by the photocurrent. The input ends need to be terminated with the line impedance (usually 50 Ω), otherwise the phase lag between the forward and the reflected backward propagating waves will limit the bandwidth. Bandwidth improvement with input termination is, however, at the expense of efficiency as half of the currents generated by the individual photodiodes are dissipated in the 50-Ω input termination. Fig. 1 shows the bandwidth-response tradeoff in a single section TWDP with and without input termination. Termination of the input with a 50-Ω load increases the bandwidth, but the response decreases by up to 6 dB.

S. Murthy, S.-J. Kim, T. Jung, T. Itoh, and M. C. Wu are with the Electrical Engineering Department, University of California, Los Angeles, CA 90095-1594 USA.

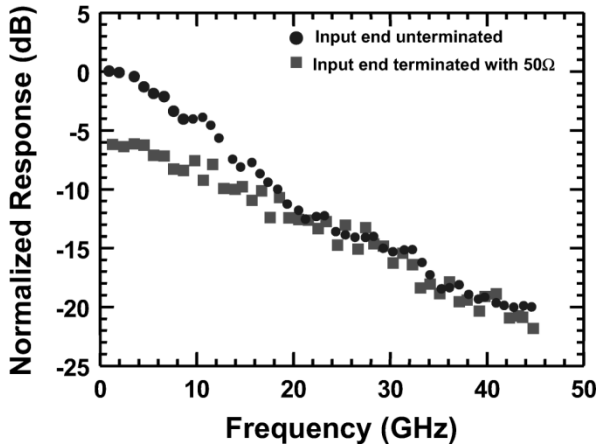Z.-Z. Wang and W. Hsin are with Demeter Technologies, El Monte, CA 91731 USA.

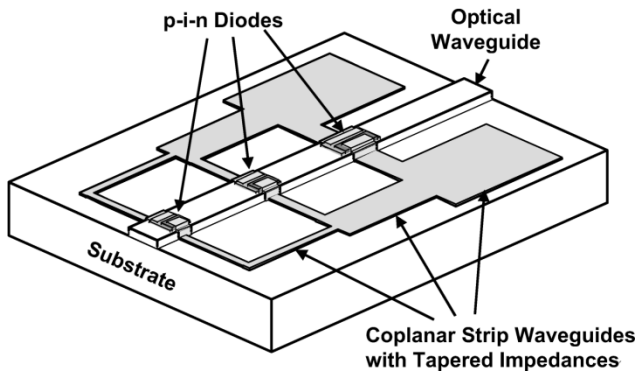Fig. 1. Effect of input termination on the frequency response of TWDP.

Fig. 2. Schematic of MS-TWDP for backward-wave cancellation.

High bandwidth without loss of responsivity can be obtained by canceling the backward propagating wave using the reflections in a multisection transmission line, as originally proposed for distributed amplification in traveling-wave tubes [16]. A similar scheme for improving the efficiency of traveling-wave distributed photodetectors has previously been proposed [17], [18] and experimentally demonstrated [19]. In this paper, we present the design, fabrication, and experimental results of a multisection transmission-line traveling-wave distributed photodetector (MS-TWDP) with dissimilar coplanar strip (CPS) sections for backward-wave cancellation. We have achieved 3-dB bandwidth of 38 GHz and up to -1 dBm of linear RF output power at 40 GHz in our photodetector.

This paper is organized as follows. In Section II, we will present the theory of backward-wave cancellation. Section III describes the design of MS-TWDP. We will present the fabrication details of the MS-TWDP device in Section IV, the measurement results in Section V, and discussions in Section VI.

II. THEORY

A. Backward-Wave Cancellation

The schematic of the proposed traveling-wave photodetector with backward-wave cancellation is shown in Fig. 2. It consists of an array of photodiodes connected by a passive optical waveguide. The photocurrents are collected in a multisection microwave transmission line. The impedance mismatch at the
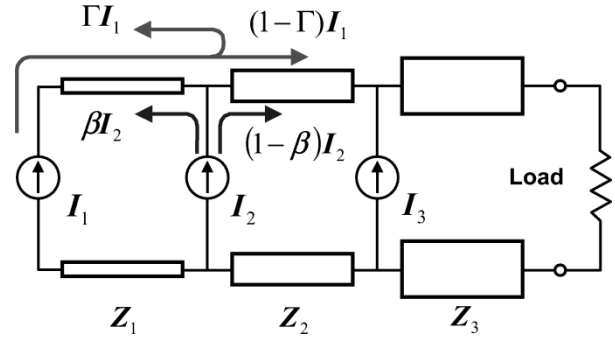

Fig. 3. Figure showing backward-wave cancellation mechanism using reflected currents at the junctions of the dissimilar transmission-line sections.

junction of the different CPS sections creates a partial reflection of the forward propagating wave. The reflection coefficient at each discontinuity is always negative provided the impedances of the multisection transmission line are tapered down toward the output end (i.e., the load). It is thus possible to use the reflected wave to cancel out the backward propagating fraction of the photocurrent generated by the photodiode at the discontinuity.

The backward-wave cancellation procedure in an MS-TWDP is shown in Fig. 3. It has three diodes generating currents $I_1, I_2,$ and I_3 into transmission lines with line impedances $Z_1, Z_2,$ and Z_3, respectively. When the current I_1 from diode 1 reaches the transmission-line section with impedance Z_2, ΓI_1 is reflected back toward the input end and $(1 - \Gamma)I_1$ is transmitted toward the output load, where

$$\Gamma = \frac{Z_2 - Z_1}{Z_2 + Z_1} \tag{1}$$

is the reflection coefficient. The current I_2 from diode 2, on the other hand, divides into two parts: βI_2 flows toward the input end and $(1 - \beta)I_2$ flows toward the output end, where

$$\beta = \frac{Z_2}{Z_1 + Z_2}. \tag{2}$$

To cancel the backward propagating wave, the line impedances Z_1 and Z_2 should be chosen such that

$$\Gamma I_1 + \beta I_2 = 0. \tag{3}$$

Substituting (1) and (2) into (3), we obtain

$$\frac{Z_2}{Z_1} = \frac{I_1}{I_1 + I_2}. \tag{4}$$

In general, the relation between the line impedance of the adjacent sections can be derived to be

$$\frac{Z_{n+1}}{Z_n} = \frac{\sum_{j=1}^{n+1} I_j}{\sum_{i=1}^{n} I_i} \tag{5}$$

where Z_n and Z_{n+1} are the impedances of the nth and $n+1$th sections (with suffix n increasing from input end to output end), and I_i refers to the photocurrent generated by the ith diode. The above relation can be used to design the impedances of the
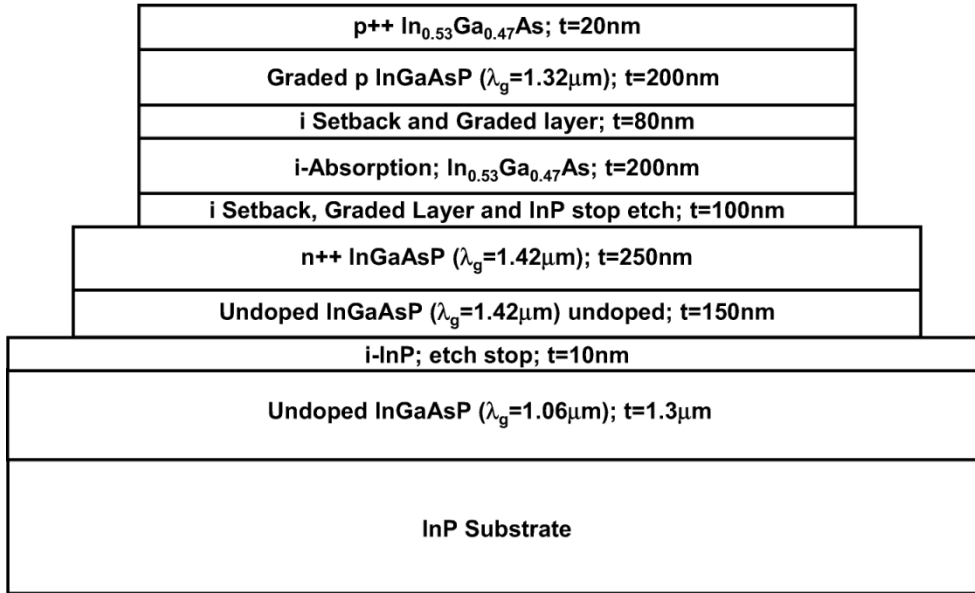
Fig. 4. Epitaxial structure used for the fabrication of MS-TWDP.

different section of the multisection transmission line for any arbitrary distribution of currents among the individual diodes of the MS-TWDP. For the case when the currents generated by all the diodes are the equal, (5) reduces to

$$Z_n = \frac{Z_1}{n}. \tag{6}$$

In (6), n increases from input to output ends, Z_n is the line impedance of the nth section looking in from the input end, and Z_1 is the impedance of the input section. We have previously demonstrated backward-wave cancellation for unequal current distribution among the diodes of the photodetector [19]. In this paper, we will present a design with equal photocurrent distribution among the diodes.

B. Frequency Response of TWDP

Frequency response of the MS-TWDP is calculated using the ABCD matrices for the individual diode and transmission-line sections as shown in Fig. 3 [7]. The voltages and currents at the terminals of the unit cells are evaluated recursively to get the general solution, using

$$\begin{bmatrix} V_{n+1} \\ I_{n+1} \end{bmatrix} = M_{cs}^n \cdot M_d^n \cdot \begin{bmatrix} V_n \\ I_n \end{bmatrix} + \begin{bmatrix} 0 \\ i_n \end{bmatrix} \exp[-j\beta_{opt}(f)(l_{cs}+l_d)n]$$
$$\times \frac{1}{1+j\omega R_d^n C_d^n} F_t(j\omega) \quad (7)$$

where V_n and I_n are the voltage and current at the nth unit cell, M_{cs}^n and M_d^n are the ABCD matrix elements [21] for the nth coplanar section and diode, respectively, i_n is the current generated by the nth diode, β_{opt} is the propagation constant of the optical wave, l_{cs} is the length of the coplanar transmission line between two diodes, l_d is the diode length, R_d^n and C_d^n are the series resistance and the capacitance of the nth diode, and $F_t(j\omega)$ is the normalized transit-time frequency response [22].

The particular solution can be obtained from the termination conditions at the input and output using

$$\begin{bmatrix} V_N \\ I_N \end{bmatrix} = \begin{bmatrix} V_N' \\ I_N' \end{bmatrix} + M_d^1 \cdot \prod_{n=2}^N (M_{cs}^n \cdot M_d^n)$$
$$\cdot \begin{bmatrix} 1 \\ -\frac{1}{Z_{in0}} \end{bmatrix} \cdot V_0 \tag{8}$$

$$\frac{V_N}{I_N} = Z_{out} \tag{9}$$

where N is the total number of diodes, V_N' and I_N' are the general solution values for the voltage and current at the Nth unit cell, Z_{in} is the input termination, and Z_{out} is the output termination. If we define

$$M = M_d^1 \cdot \prod_{n=2}^N (M_{cs}^n \cdot M_d^n) = \begin{pmatrix} M_{11} & M_{12} \\ M_{21} & M_{22} \end{pmatrix} \tag{10}$$

then V_0 can be expressed as

$$V_0 = \frac{V_N' - Z_{out} I_N'}{Z_{out}\left(M_{21} - \frac{M_{22}}{Z_{in}}\right) - \left(M_{11} - \frac{M_{12}}{Z_{in}}\right)}. \tag{11}$$

The output current can be found by solving I_N.

III. PHOTODETECTOR DESIGN

A. Microwave Design

The first step is to choose the fractional current generated in the individual diodes and the number of diodes in the photodetector. We would ideally like to have equal currents in the individual photodiodes so the maximum photocurrent is not limited by thermal failure of the first diode [15], [23]. In practice, the number of diodes will be limited by the maximum line impedance that can be microfabricated on chip and microwave losses of the skinniest (highest impedance) line. The first CPS section in MS-VMDP has the highest line impedance, which
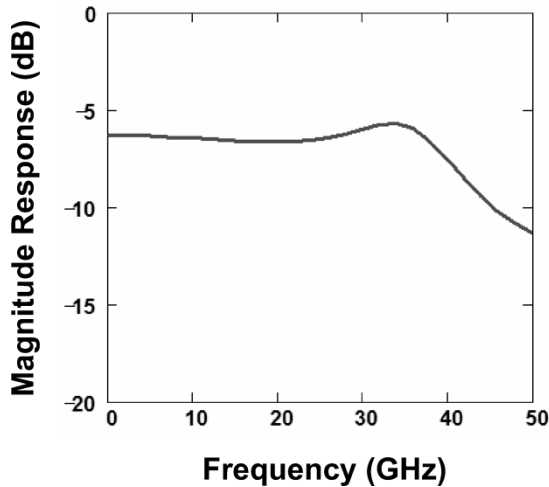
Fig. 5. Simulated frequency response of our MS-TWDP design with three diodes.
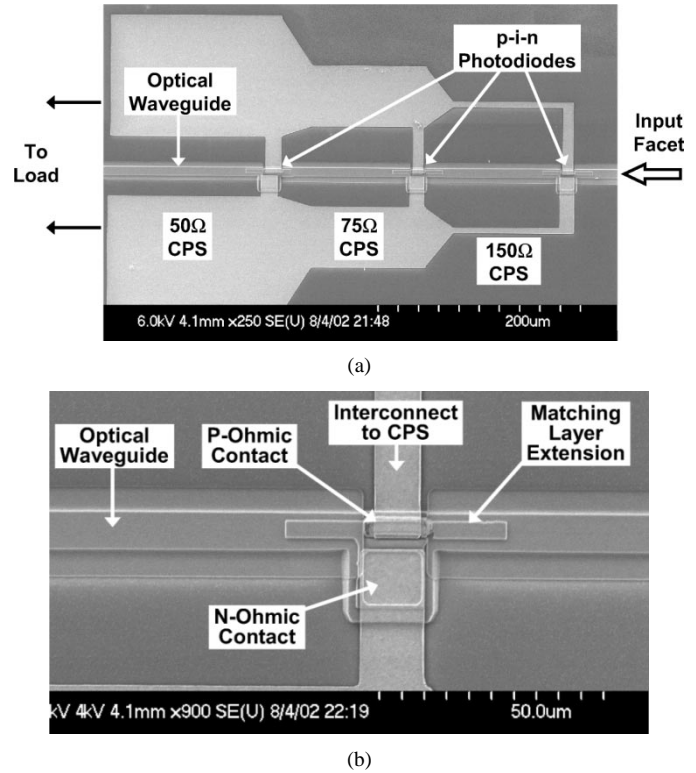

(a)

(b)

Fig. 6. (a) SEM of the fabricated photodetector showing the three p-i-n diodes and the different coplanar strip sections. (b) Closeup view of the p-i-n photodiode and the matching layer extension on passive waveguide.

equals the number of diodes multiplied by the output impedance of the photodetector. In this paper, we choose to use three discrete diodes with equal photocurrent distribution. The required line impedances of the individual sections of the multisection transmission line are thus 150, 75, and 50 Ω [(6)] from input to output. The widths of the coplanar lines are 2, 40, and 120 μm, and the separations between signal and ground electrodes are 120, 100, and 60 μm, respectively [24]. The spacing between the diodes is designed to be 300 μm to obtain the desired loaded line impedances of 150, 75, and 50 Ω for the three sections (the input section is 150 Ω, and the output section is 50 Ω).

B. Epitaxial Layer Design

In a series feed photodetector, the maximum linear photocurrent is limited either by thermally induced failure or charge screening due to high photocurrent densities. In either case the entire photodetector ends up being limited by the diode with highest photocurrent or photocurrent densities. It is desirable to have uniform photocurrent distribution among individual photodiodes. Equal photocurrents and photocurrent densities can be obtained through parallel feed of the diodes with an integrated multimode interference (MMI) coupler [20]. The MMI coupler however increases the size of the photodetector. In this paper, equal photocurrents are achieved by tailoring the lengths of the photodiodes. The epitaxial layer structure is shown in Fig. 4. The main structure consists of a 1.3-μm-thick passive waveguide layer (quaternary layer with bandgap wavelength λ_g of 1.06 μm) and a 0.2-μm-thick InGaAs absorption layer. A 0.4-μm-thick InGaAsP ($\lambda_g = 1.42$ μm) matching layer is inserted between the passive waveguide and the absorption region to enhance the optical coupling. The extension of the matching layer beyond the diode can be optimized for high responsivity [25] or for high linearity [26]. The lengths of the diodes in our photodetector are 8, 10, and 20 μm, respectively. The matching layer extension is chosen to be 18 μm for high linearity. The undoped setback layers on either side of the absorbing region are graded to reduce carrier trapping and increase bandwidth. The upper half of the matching layer is doped to form the n-contact layer. The lower half is not doped to reduce optical losses in
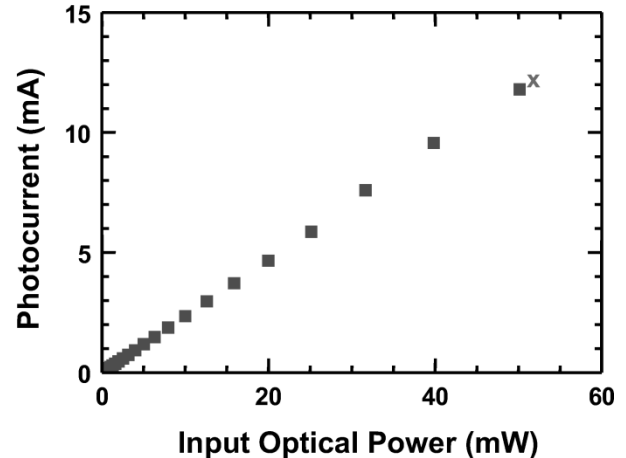
Fig. 7. DC responsivity measurement. DC photocurrent is linear up to 12 mA at −4 V bias.

the passive waveguide. The theoretical frequency response for the MS-TWDP, calculated using the formulation in Section II, is shown in Fig. 5. The 3-dB bandwidth is 42 GHz, limited by the velocity mismatch between microwave and optical signals.

IV. DEVICE FABRICATION

A 4-μm-wide active mesa is first selectively wet-etched using the H_2SO_4:H_2O_2:$10H_2O$ solution. The n-contact mesa and the matching layer are then patterned using the same H_2SO_4:H_2O_2:$10H_2O$ etchant. The p-contact is patterned on the active mesa by evaporating 200 Å AuZn/300 Å Ti/2000 Å Au in an electron-beam evaporator followed by conventional
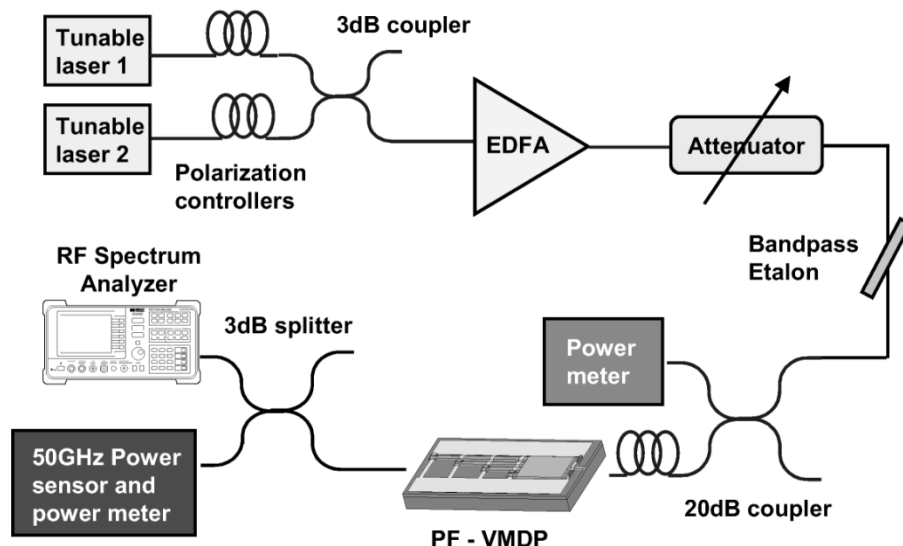
Fig. 8. Heterodyne setup for RF linearity measurement.

photoresist liftoff in acetone. The 0.7-μm-high 12-μm-wide rib waveguides are formed in the InGaAsP ($\lambda_g = 1.06\ \mu$m) layer by time etching in HCl:HNO$_3$:H$_2$O. Next, 5000 Å of Si$_3$N$_4$ is deposited at 325°C by plasma-enhanced chemical vapor deposition to passivate the photodiodes. Windows are opened in the nitride for n-contacts and interconnect metals. Finally, 50 Å Ni/1000 Å AuGe/1000 Å Ag/2000 Å Au is patterned using e-beam evaporation and liftoff processes. The n-ohmic metal is also used as the interconnect metal to save a mask step in the fabrication of the device. The contacts are annealed using a rapid thermal processor system at 380 °C for 10 s. The scanning electron micrograph (SEM) of a fabricated device is shown in Fig. 6(a). Fig. 6(b) shows a closeup view of the active photodiodes. The 18-μm-long match layer extensions on both sides of the photodiode are clearly observed.

V. RESULTS AND DISCUSSION

The dc responsivity of the MS-TWPD is 0.24 A/W (Fig. 7). The responsivity is limited by the losses at the waveguide–photodiode interface, fiber coupling loss into the optical waveguide, and imperfections in the anti-reflection coating. The matching layer and the photodiode sections are multimode waveguides. The coupling loss between the passive waveguide and the absorption region is estimated to be 15% per interface using beam propagation method simulations. The dark current is less than 100 nA per diode and a bias of -2 V is sufficient to completely deplete the absorption layer. The dc responsivity, shown in Fig. 7, remains linear up to 12 mA, at which point the thin metal interconnect between the first photodiode and the microwave transmission line is damaged. After failure, the detector responsivity is decreased by $\sim$30 % but remains operational. The heterodyne frequency measurement setup used for bandwidth and RF linearity measurements is shown in Fig. 8. Two Photonetics external cavity tunable diode lasers are mixed to generate the RF signal. The combined optical signal is amplified in an SDL FA30 erbium-doped fiber amplifier (EDFA) and then coupled into the MS-TWPD using a lensed fiber. The input optical power is controlled by an variable optical attenuator. An
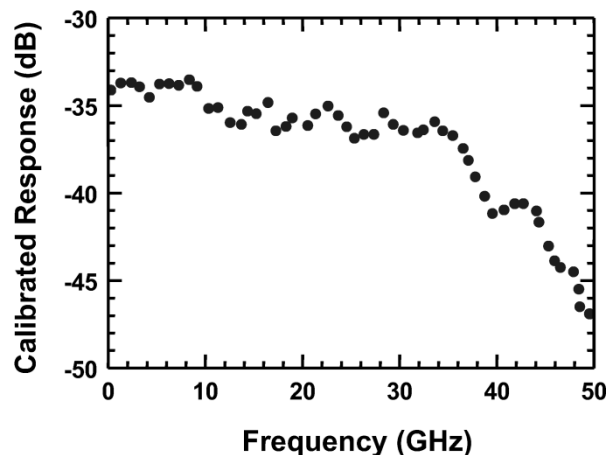

Fig. 9. Frequency response of the MS-TWDP photodetector. The 30-dB bandwidth is 38 GHz.

optical bandpass filter with 5-nm bandwidth is inserted to reject the out-of-band optical power from the EDFA output. The generated RF signal is collected by probing the 50-Ω section of the MS-TWDP with a 40-GHz GGB Industries picoprobe and measured in an Agilent 8487A power sensor-power meter. The RF frequency is monitored throughout the measurement using an Agilent 8565E RF spectrum analyzer. The measured RF power increases quadratically with the input optical power.

The frequency response measured at 0 dBm input optical power and -2 V bias is shown in Fig. 9. The 3-dB bandwidth is 38 GHz. It should be mentioned that the frequency response of the probe, which, per specifications, has a loss of 1 dB at 40 GHz, has not been calibrated out of this measurement. In spite of this, the measured bandwidth is 2.5 times higher than the round-trip time bandwidth limit of 15 GHz. This confirms that the backward-wave in our MS-TWPD is indeed cancelled. Backward-wave cancellation enables us to achieve high bandwidth in traveling-wave distributed photodetectors without losing 6 dB of electrical power in the input termination resistor. With backward-wave cancellation, the necessity of fabricating an on-chip termination resistor and dc blocking capacitor no
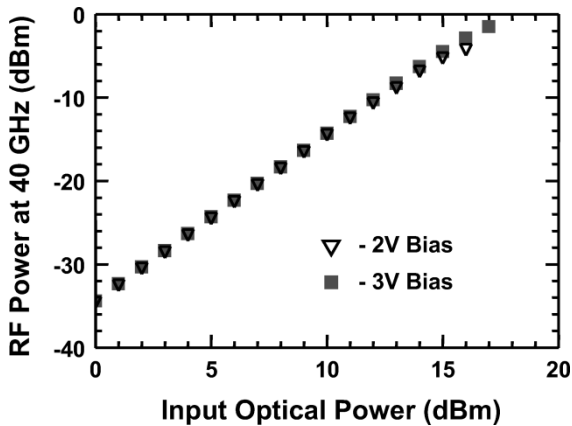
Fig. 10. RF linearity measurement at 40 GHz. RF output at 40 GHz remains linear up to −1 dBm.

longer exists, simplifying the fabrication process. The linearity measurement of the RF response at 40 GHz is shown in Fig. 10. At a bias of −2 V, the 40-GHz RF response compresses by 1 dB at −5 dBm. When the bias voltage is increased to −3 V, the 1-dB compression power increases to −1 dBm. When the bias was further increased to −4 V, the first diode of the detector failed (indicated by the reduction of the photodetector responsivity by 30%). The failure is due to thermal dissipation induced disconnection of the interconnect metal from the diode contacts. With thicker metal interconnects and improved heat sinking, we expect to achieve even higher linear RF powers.

VI. CONCLUSION

We have successfully designed and fabricated a traveling-wave photodetector with backward-wave cancellation structures. The total absorption length of 38 μm is divided into three discrete photodiodes spaced by 300 μm. The lengths of the diodes (8, 10, and 20 μm) are chosen to achieve uniform photocurrent distribution. The photodiodes are connected by a passive optical waveguide, and output signals are collected by multisection coplanar strips with step-reduced impedances. Cancellation of backward propagating waves is confirmed experimentally. The 3-dB frequency is measured to be 38 GHz. A maximum linear photocurrent of 12 mA is achieved at dc. A maximum linear RF power of −1 dBm is observed at 40 GHz using optical heterodyne technique. Higher linear photocurrent could be obtained by increasing the thickness of the metal interconnect lines. We have also reported a theoretical model for the backward-wave-cancelled traveling-wave photodetectors. Good agreements between theoretical and experimental results have been achieved. This photodetector is useful for analog fiber-optic links and RF photonic systems.

REFERENCES

[1] H. F. Taylor, O. Eknoyan, C. S. Park, K. N. Choi, and K. Chang, "Traveling-wave photodetectors," in *Proc. SPIE*, vol. 1217, 1990, pp. 59–63.
[2] D. Jager, M. Block, D. Kaiser, M. Welters, and W. von Wendorff, "Wave propagation phenomena and microwave-optical interaction in coplanar lines on semiconductor substrate," *J. Electromagn. Waves Applicat.*, vol. 5, no. 4–5, pp. 337–351, 1991.
[3] K. S. Giboney, M. J. W. Rodwell, and J. E. Bowers, "Traveling-wave photodetectors," *IEEE Photon. Technol. Lett.*, vol. 4, pp. 1363–1365, Dec. 1992.
[4] V. M. Hietala, G. A. Vawter, T. M. Brennan, and B. E. Hammons, "Traveling-wave photodetectors for high-power, large-bandwidth applications," *IEEE Trans. Microwave Theory Tech.*, pt. 2, vol. 43, pp. 2291–2298, Sept. 1995.
[5] L. Y. Lin, M. C. Wu, T. Itoh, T. A. Vang, R. E. Muller, D. L. Sivco, and A. Y. Cho, "Velocity-matched distributed photodetectors with high-saturation power and large bandwidth," *IEEE Photon. Technol. Lett.*, vol. 8, pp. 1376–1378, Oct. 1996.
[6] K. S. Giboney, J. W. Rodwell, and J. E. Bowers, "Traveling-wave photodetector theory," *IEEE Trans. Microwave Theory Tech.*, pt. 2, vol. 45, pp. 1310–1119, Aug. 1997.
[7] L. Y. Lin, M. C. Wu, T. Itoh, T. A. Vang, R. E. Muller, D. L. Sivco, and A. Y. Cho, "High-power high-speed photodetectors-design, analysis, and experimental demonstration," *IEEE Trans. Microwave Theory Tech.*, pt. 2, vol. 45, pp. 1320–1331, Aug. 1997.
[8] E. Droge, E. H. Bottcher, S. Kollakowski, A. Strittmatter, D. Bimberg, O. Reimann, and R. Steingruber, "78 GHz distributed InGaAs MSM photodetector," *Electron. Lett.*, vol. 34, no. 23, 12, pp. 2241–2243, Nov. 1998.
[9] A. Stohr, R. Heinzelmann, A. Malcoci, and D. Jager, "Optical heterodyne millimeter-wave generation using 1.55-μm traveling-wave photodetectors," *IEEE Trans. Microwave Theory Tech.*, pt. 2, vol. 49, pp. 1926–1933, Oct. 2001.
[10] Y. Hirota, T. Ishibashi, and H. Ito, "1.55-μm wavelength periodic traveling-wave photodetector fabricated using unitraveling-carrier photodiode structures," *J. Lightwave Technol.*, vol. 19, pp. 1751–1758, Nov. 2001.
[11] M. S. Islam, S. Murthy, T. Itoh, M. C. Wu, D. Novak, R. B. Waterhouse, D. L. Sivco, and A. Y. Cho, "Velocity-matched distributed photodetectors and balanced photodetectors with p-i-n photodiodes," *IEEE Trans. Microwave Theory Tech.*, pt. 2, vol. 49, pp. 1914–1920, Oct. 2001.
[12] J.-W. Shi, K.-G. Gan, Y.-H. Chen, C.-K. Sun, Y.-J. Chiu, and J. E. Bowers, "Ultrahigh-power-bandwidth product and nonlinear photo-conductance performances of low-temperature-grown GaAs-based metal-semiconductor-metal traveling-wave photodetectors," *IEEE Photon. Technol. Lett.*, vol. 14, pp. 1587–1589, Nov. 2002.
[13] A. Stohr, A. Malcoci, F. Siebe, K. Lill, P. van der Waal, R. Gusten, and D. Jager, "Integrated photonic THz transmitter employing ultra-broad-band travelling-wave 1.55 μm photodetectors," *Int. Topical Meeting Microwave Photonics 2002*, pp. 69–72, Nov. 2002.
[14] C. H. Cox, "Gain and noise figure in analogue fiber-optic links," *Proc. Inst. Elect. Eng. J*, vol. 139, no. 4, pp. 238–242, 1992.
[15] A. Nespola, T. Chau, M. C. Wu, and G. Ghione, "Analysis of failure mechanisms in velocity-matched distributed photodetectors," *Proc. Inst. Elect. Eng. Optoelectronics*, vol. 146, no. 1, pp. 25–30, Feb. 1999.
[16] E. L. Ginzton, W. R. Hewlett, J. H. Jasberg, and J. D. Noe, "Distributed amplification," in *Proc. IRE*, vol. 36, Aug. 1948, pp. 956–969.
[17] M. P. Nesnidal, A. C. Davidson, G. R. Emmel, R. A. Marsland, and M. C. Wu, "Efficient, reliable, high-power VMDPs for linear fiber optic signal transmission," in *Proc. PSAA-10*, Monterey, CA, Feb. 16–17, 2000.
[18] J.-W. Shi, C.-K. Sun, and J. E. Bowers, "Taper line distributed photodetector," in *Tech. Dig. LEOS 2001*, San Diego, CA, Nov. 11–15, pp. 382–383.
[19] S. Murthy, T. Jung, M. C. Wu, D. L. Sivco, and A. Y. Cho, "Traveling-wave distributed photodetectors with backward-wave cancellation for improved AC efficiency," *Electron. Lett.*, vol. 38, no. 15, pp. 827–829, July 2002.
[20] S. Murthy, M. C. Wu, D. L. Sivco, and A. Y. Cho, "Parallel feed traveling-wave distributed pin photodetectors with integrated MMI couplers," *Electron. Lett.*, vol. 38, no. 2, pp. 78–80, Jan. 17, 2002.
[21] D. Pozar, *Microwave Engineering*, 2nd ed: Wiley, 1998, pp. 206–209.
[22] J. E. Bowers and C. A. Burrus, "Ultrawide-band long-wavelength p-i-n photodetectors," *J. Lightwave Technol.*, vol. LT-5, pp. 1339–1350, Oct. 1987.
[23] M. S. Islam, T. Jung, T. Itoh, M. C. Wu, A. Nespola, D. L. Sivco, and A. Y. Cho, "High power and highly linear monolithically integrated distributed balanced photodetectors," *J. Lightwave Technol.*, vol. 20, pp. 285–295, Feb. 2002.
[24] K. C. Gupta, R. Garg, I. Bahl, and P. Bhartia, *Microstrip Lines and Slotlines*, pp. 375–422, 1996.
[25] R. J. Hawkins, R. J. Deri, and O. Wada, "Optical power transfer in vertically integrated impedance-matched waveguide/photodetectors: Physics and implications for diode-length reduction," *Opt. Lett.*, vol. 16, no. 7, pp. 470–472, Apr. 1, 1991.
[26] S. Murthy, T. Jung, M. C. Wu, Z. Wang, and W. Hsin, "Linearity improvement in photodetectors by using index-matching layer extensions," presented at the LEOS 2002, Glasgow, Scotland, Nov. 10–14.

Sanjeev Murthy (S'98) received the B.Tech. degree in electronics and communication engineering from the Indian Institute of Technology, Madras, in 1994 and the M.S. degree in electrical engineering from the University of California, Los Angeles (UCLA), in 1999. He is currently working toward the Ph.D. degree in electrical engineering at UCLA. His dissertation work includes integrating multimode interference couplers with velocity-matched distributed and backward-wave cancellation in distributed photodetectors to achieve high-power and high bandwidth.

His other research interests include waveguide devices, integrated optoelectronic devices, integrated microwave photonic devices, and mode-locked lasers.

Seong-Jin Kim, photograph and biography not available at the time of publication.

Thomas Jung (S'03), photograph and biography not available at the time of publication.

Zhi-Zhi Wang, photograph and biography not available at the time of publication.

Wei Hsin, photograph and biography not available at the time of publication.

T. Itoh (M'69–SM'74–F'82–LF'03) received the Ph.D. degree in electrical engineering from the University of Illinois, Urbana, in 1969.

From September 1966 to April 1976, he was with the Electrical Engineering Department, University of Illinois. From April 1976 to August 1977, he was a Senior Research Engineer in the Radio Physics Laboratory, SRI International, Menlo Park, CA. From August 1977 to June 1978, he was an Associate Professor at the University of Kentucky, Lexington. In July 1978, he joined the faculty at The University of Texas at Austin, where he became a Professor of Electrical Engineering in 1981 and Director of the Electrical Engineering Research Laboratory in 1984. During summer 1979, he was a guest researcher at AEG-Telefunken, Ulm, West Germany. In September 1983, he was selected to hold the Hayden Head Centennial Professorship of Engineering at The University of Texas. In September 1984, he was appointed Associate Chairman for Research and Planning of the Electrical and Computer Engineering Department at The University of Texas. In January 1991, he joined the University of California, Los Angeles (UCLA), as Professor of Electrical Engineering and holder of the TRW Endowed Chair in Microwave and Millimeter Wave Electronics. He was an Honorary Visiting Professor at Nanjing Institute of Technology, China, and at the Japan Defense Academy. In April 1994, he was appointed as Adjunct Research Officer for the Communications Research Laboratory, Ministry of Post and Telecommunication, Japan. He currently holds Visiting Professorship at University of Leeds, U.K. He has 310 journal publications and 640 refereed conference presentations and has written 30 books/book chapters in the area of microwaves, millimeter waves, antennas, and numerical electromagnetics. He has also generated 60 Ph.D. students.

Dr. Itoh is a Member of the Institute of Electronics and Communication Engineers of Japan and Commissions B and D of USNC/URSI and was elected Member of the National Academy of Engineering in 2003. He was elected as an Honorary Life Member of the MTT Society in 1994. He was the Chairman of USNC/URSI Commission D from 1988 to 1990 and Chairman of Commission D of the International URSI from 1993 to 1996. He currently serves on the Administrative Committee of IEEE Microwave Theory and Techniques Society and was the Microwave Theory and Techniques Society Vice President (1989) and President (1990). He is currently Chair of the Long Range Planning Committee of URSI and serves on the advisory boards and committees of a number of organizations. He has received a number of awards, including the Shida Award from the Japanese Ministry of Post and Telecommunications in 1998, the Japan Microwave Prize in 1998, the IEEE Third Millennium Medal in 2000, and the IEEE MTT Distinguished Educator Award in 2000. He served as the Editor of IEEE TRANSACTIONS ON MICROWAVE THEORY AND TECHNIQUES from 1983 to 1985, and he was the Editor-in-Chief of IEEE MICROWAVE AND GUIDED WAVE LETTERS from 1991 to 1994.

Ming C. Wu (S'82–M'83–SM'00–F'02) received the B.S. degree in electrical engineering from the National Taiwan University in 1983 and the M.S. and Ph.D. degrees in electrical engineering from the University of California, Berkeley, in 1985 and 1988, respectively.

From 1988 to 1992, he was a Member of the Technical Staff at AT&T Bell Laboratories, Murray Hill, NJ. In 1993, he joined the Faculty of the Electrical Engineering Department of the University of California, Los Angeles (UCLA), where he is currently a Professor. He is also Director of UCLA's Nanoelectronics Research Facility and Vice Chair for Industrial Relations. He has published more than 360 papers, contributed four book chapters, and holds 11 U.S. patents. His current research interests include microelectromechanical systems (MEMS), optical MEMS (MOEMS), biophotonics, microwave photonics, and high-speed optoelectronics.

Dr. Wu is a David and Lucile Packard Foundation Fellow (1992–1997). He was the founding Co-Chair of the IEEE LEOS Summer Topical Meeting on Optical MEMS in 1996, which has now evolved into the IEEE which is held alternatively in Europe, Asia, and the United States. He has also served on the program committees of many other conferences, including Optical Fiber Communication (OFC), the Conference on Lasers and Electro-Optics (CLEO), the IEEE Conference on Micro Electro Mechanical Systems (MEMS), Lasers & Electro-Optics Society (LEOS) annual meetings, the International Electron Device Meeting (IEDM), the Device Research Conference (DRC), the International Solid-State Circuit Conference (ISSCC), and Microwave Photonics (MWP) conferences.